
RVLM: RECURSIVE VISION-LANGUAGE MODELS WITH ADAPTIVE DEPTH

A PREPRINT

✉ **Nicanor Mayumu**

Department of Computer Science
University of Wollongong in Dubai
Dubai Knowledge Park, Dubai, UAE
nngwanga@uow.edu.au

✉ **Zeenath Khan**

Department of Computer Science
University of Wollongong in Dubai
Dubai Knowledge Park, Dubai, UAE
ZeenathKhan@uowdubai.ac.ae

✉ **Melodena Stephens**

Department of Academic Affairs
Mohammed Bin Rashid School of Government
City Walk, Building B02, Dubai, UAE
melodena.stephens@mbrsg.ac.ae

✉ **Patrick Mukala**

Department of Computer Science
University of Wollongong in Dubai
Dubai Knowledge Park, Dubai, UAE
PatrickMukala@uowdubai.ac.ae

✉ **Farhad Oroumchian**

Department of Computer Science
University of Wollongong in Dubai
Dubai Knowledge Park, Dubai, UAE
FarhadOroumchian@uowdubai.ac.ae

ABSTRACT

Medical AI systems face two fundamental limitations. First, conventional vision-language models (VLMs) perform single-pass inference, yielding black-box predictions that cannot be audited or explained in clinical terms. Second, iterative reasoning systems that expose intermediate steps rely on fixed iteration budgets wasting compute on simple cases while providing insufficient depth for complex ones. We address both limitations with a unified framework. RVLM replaces single-pass inference with an iterative generate-execute loop: at each step, the model writes Python code, invokes vision sub-agents, manipulates images, and accumulates evidence. Every diagnostic claim is grounded in executable code, satisfying auditability requirements of clinical AI governance frameworks. RRoumchian makes iteration depth adaptive: a lightweight controller predicts the optimal budget from task-complexity features, then monitors progress and terminates early when reasoning stalls. We evaluate on BraTS 2023 Meningioma (brain MRI) and MIMIC-CXR (chest X-ray) using Gemini 2.5 Flash without fine-tuning. Across repeated runs, RVLM shows high consistency on salient findings (e.g., mass presence and enhancement) and can detect cross-modal discrepancies between Fluid-Attenuated Inversion Recovery (FLAIR) signal characteristics and segmentation boundaries. On MIMIC-CXR, it generates structured reports and correctly recognises view-specific artefacts. Code: <https://github.com/nican2018/rvlm>.

Keywords Vision Language Models · Recursive Reasoning · Adaptive Computation · Medical Imaging · REPL · Interpretability · Chest X-Ray · Brain MRI

1 Introduction

The integration of artificial intelligence into clinical radiology has progressed rapidly, with vision-language models (VLMs) demonstrating impressive capabilities in tasks ranging from lesion detection to automated report genera-

tion [Singhal et al., 2022, AJ et al., 2023]. These models can process multimodal inputs medical images alongside textual prompts and produce diagnostic outputs that increasingly approach clinical expert performance. Yet despite these technical advances, widespread adoption in high-stakes clinical settings remains elusive. Two fundamental limitations persist: the opacity of model reasoning and the inflexibility of computational resource allocation.

1.1 The Interpretability Challenge

Current medical VLMs operate predominantly as single-pass inference systems. Given an image and a prompt, they produce a diagnosis or report in one forward pass, revealing none of the intermediate reasoning that led to the conclusion. This black-box nature conflicts directly with the evidentiary standards of clinical medicine [Ghassemi et al., 2021]. When a radiologist interprets a study, they can articulate which anatomical structures were examined, what features supported or contradicted each differential diagnosis, and how quantitative measurements informed their assessment. A clinician using an AI system requires the same transparency: the ability to audit, verify, and if necessary, challenge the model’s reasoning [Raji et al., 2020, Thieme et al., 2023].

The consequences of opaque AI in medicine extend beyond clinician distrust. Regulatory frameworks increasingly mandate transparency. The EU AI Act classifies medical AI as high-risk, requiring systems to provide meaningful explanations of their decisions and enable human oversight. ISO/IEC 42001 and the NIST AI Risk Management Framework similarly emphasise traceability, reproducibility, and auditability. Current VLMs, designed for benchmark performance rather than regulatory compliance, cannot meet these requirements.

1.2 The Fixed-Budget Problem

A second limitation compounds the first. Recent work has explored iterative reasoning systems that do expose intermediate steps: chain-of-thought prompting, REPL-based execution, and agentic frameworks that decompose problems into subtasks. These systems improve interpretability by revealing the model’s step-by-step reasoning. However, they universally rely on a *fixed iteration budget*, a user-specified `max_iterations` hyperparameter applied uniformly across all cases regardless of diagnostic complexity.

This one-size-fits-all approach creates a dilemma. A simple case, a single well-defined meningioma with clear boundaries, may require only three reasoning steps: identify the lesion, measure its dimensions, characterise its appearance. Allocating a fixed budget of twelve iterations wastes computational resources, increases API costs, and adds unnecessary latency. Conversely, a complex case, a multifocal tumour with ambiguous margins, peritumoural oedema, and heterogeneous enhancement *benefits* from additional iterations to resolve uncertainty, consult multiple views, and cross-validate findings. A fixed budget either under-serves complex cases or over-serves simple ones. The optimal number of reasoning steps is a property of the task, not the system, yet existing architectures cannot adapt.

1.3 Our Contributions

We address both limitations simultaneously through a unified framework combining two complementary components. **RVLM** (Recursive Vision-Language Model) provides the interpretability layer, replacing single-pass inference with an iterative generate-execute loop where reasoning unfolds step by step in executable code. **RECURSIONROUTER** makes iteration depth itself adaptive, predicting case complexity and terminating reasoning when progress stalls.

Specifically, this paper makes the following contributions:

- We extend the RLM REPL framework [Zhang et al., 2026] with first-class image support, introducing primitives for visual reasoning: `context_images` for maintaining multimodal working memory, `describe_image` for generating natural language descriptions of regions of interest, `llm_query_with_images` for visual question answering, and programmatic image manipulation functions (crop, enhance, difference maps). The model accumulates evidence across iterations, building a verifiable reasoning trace where every claim corresponds to executable code.
- We introduce a pre-flight complexity estimator that predicts optimal iteration depth from task features (label entropy, tumour volume, sub-region count, presence of tiny regions) and a per-iteration stall detector that monitors reasoning progress. This treats recursion depth as a latent variable inferred from the input, eliminating the fixed-budget hyperparameter entirely.
- We provide an explicit mapping from RVLM’s mechanisms to the requirements of clinical AI governance. The system’s executable traces directly satisfy EU AI Act transparency obligations, ISO/IEC 42001 traceability requirements, and NIST AI RMF principles of explainability and human oversight. We argue that interpretability must be architected in, not added post-hoc.

- Recognising that executable code is not a clinician-friendly output, we implement a secondary LLM pass that converts RVLM’s reasoning traces into formal, structured patient reports in PDF format. This abstraction layer maintains the verifiability of the underlying code while presenting information in the familiar style of radiology documentation.
- We evaluate the combined system on two clinically distinct benchmarks without task-specific fine-tuning. On BraTS 2023 Meningioma (brain MRI with four modalities and segmentation overlays), RVLM achieves 90% consistency on high-salience findings across 16 independent runs and autonomously detects cross-modal discrepancies absent from single-pass baselines. On MIMIC-CXR (chest radiography with PA/Lateral/AP views), the same infrastructure generates structured Findings and Impression reports, correctly recognising view-specific artefacts and producing clinically coherent documentation.

1.4 Precision-Latency-Complexity Tradeoff

RVLM explicitly prioritises *verifiability* and *transparency* over raw inference speed. The system is designed not to replace real-time screening tools, but to serve as a complementary technology for high-stakes scenarios where reasoning matters as much as results: second-opinion systems for complex cases, research validation pipelines, pre-operative planning, and radiology education. RECURSIONROUTER recovers efficiency where possible by matching computational investment to case difficulty, ensuring that the system’s latency reflects the complexity of the diagnostic task.

1.5 Paper Organisation

The remainder of this paper is organised as follows. Section 2 reviews related work in medical VLMs, iterative reasoning systems, and adaptive computation. Section 3 details the RVLM architecture, including the REPL environment, vision primitives, and state management. Section 4 introduces RECURSIONROUTER and its complexity prediction and stall detection mechanisms. Section 5 maps the architecture to regulatory trust frameworks, providing a concrete pathway to compliance. Section 6 presents experimental setup and results on BraTS 2023 Meningioma and MIMIC-CXR. Section 7 analyses clinical implications, limitations, and future directions. Section 8 concludes.

2 Related Work

Vision-Language Models (VLMs). Large-scale VLMs such as GPT-4o [OpenAI, 2024], Gemini [Team et al., 2025], Claude 3.5 [Anthropic, 2024], and the LLaVA family [Liu et al., 2023, Li et al., 2024] achieve impressive performance across visual understanding, captioning, and multimodal reasoning [Mayumu et al. 2025]. These models predominantly rely on single-pass inference; the entire visual and textual reasoning must be compressed into one forward pass. Recent efforts introduce visual chain-of-thought [Zhang et al., 2024, Shao et al., 2024] and multi-turn strategies, yet these approaches lack persistent state management and do not support programmatic control over visual processing.

Recursive and iterative language model frameworks. The Recursive Language Model (RLM) paradigm [Zhang et al., 2026] embeds a language model inside a persistent REPL, enabling recursive text manipulation and long-horizon reasoning through stateful code execution. Related iterative frameworks include ReAct [Yao et al., 2023], Reflexion [Shinn et al., 2023], THREAD [Schroeder et al., 2025], and LADDER [Simonds and Yoshiyama, 2025]. None natively incorporates vision capabilities or supports recursive image manipulation.

Code-augmented and programmatic visual reasoning. ViperGPT [Surís et al., 2023] pioneered program synthesis for visual QA by composing modular visual primitives. CodeAct [Wang et al., 2024], Visual Program [Shlapentokh-Rothman et al., 2025], and Visual Chain-of-Code [Wang et al., 2025] further demonstrated that executable code reduces hallucination in vision tasks. RVLM extends this direction with (1) a *persistent, stateful REPL* enabling iterative refinement, and (2) *recursive sub-VLM calls* on arbitrary image subsets. Code-as-thought approaches [Chen et al., 2022, Gao et al., 2023] ground reasoning in verifiable computational steps; our REPL loop inherits this tradition and extends it to multimodal, multi-step medical imaging.

Adaptive computation. Early-exit networks [Teerapittayanon et al., 2016, Schwartz et al., 2020] and mixture-of-depths [Raposo et al., 2024] allocate variable compute per instance. PonderNet [Banino et al., 2021] treats computation steps as a latent variable trained end-to-end. RECURSIONROUTER applies analogous ideas to LLM iteration depth, using domain-specific task features rather than learned internal states, a practical advantage when outcome labels are scarce.

Medical vision-language models and trustworthy AI. Med-PaLM M [Tu et al., 2023], LLaVA-Med [Li et al., 2023], Med-Gemini [Saab et al., 2024], and XrayGLM [Thawakar et al., 2025] demonstrate strong radiology performance but

inherit the single-pass limitation. Trustworthy medical AI research emphasises explainability [Selvaraju et al., 2019] and uncertainty quantification [Obermeyer et al., 2019]; few works combine these with deep iterative visual reasoning. RVLM grounds every inference step in auditable Python code.

Radiology report generation. Automated chest radiograph report generation has evolved from template-based [Jing et al., 2017] to transformer-based [Chen et al., 2020, Miura et al., 2021] and VLM-driven [Hyland et al., 2024, Chen et al., 2024] approaches. RVLM differs by not requiring task-specific fine-tuning: the same REPL infrastructure, applied to brain MRI and chest X-ray through modality-aware prompt templates, adapts without weight updates.

BraTS challenge and brain tumour analysis. The BraTS Challenge [Menze and al., 2015, LaBella et al., 2023, Bakas et al., 2024] has served as the canonical brain tumour benchmark for over a decade. RVLM is, to our knowledge, the first approach to apply recursive, code-augmented vision-language reasoning to this challenge, moving beyond segmentation toward interpretable iterative diagnostic reasoning.

3 RVLM Methodology

3.1 Architectural Paradigm

The RVLM framework extends the Recursive Language Model paradigm [Zhang et al., 2026] to multimodal visual reasoning. Our central hypothesis is that image-based diagnostic reasoning, like textual analysis, benefits from recursive decomposition: a model capable of programmatically inspecting, manipulating, and recursively querying medical images across iterative cycles produces more verifiable and clinically auditable results than monolithic architectures constrained to single-pass inference. RVLM achieves this by embedding a vision-capable language model within a persistent visual REPL environment, enabling stateful, multi-step reasoning with procedural transparency. The overall system architecture is illustrated in Figure 1.

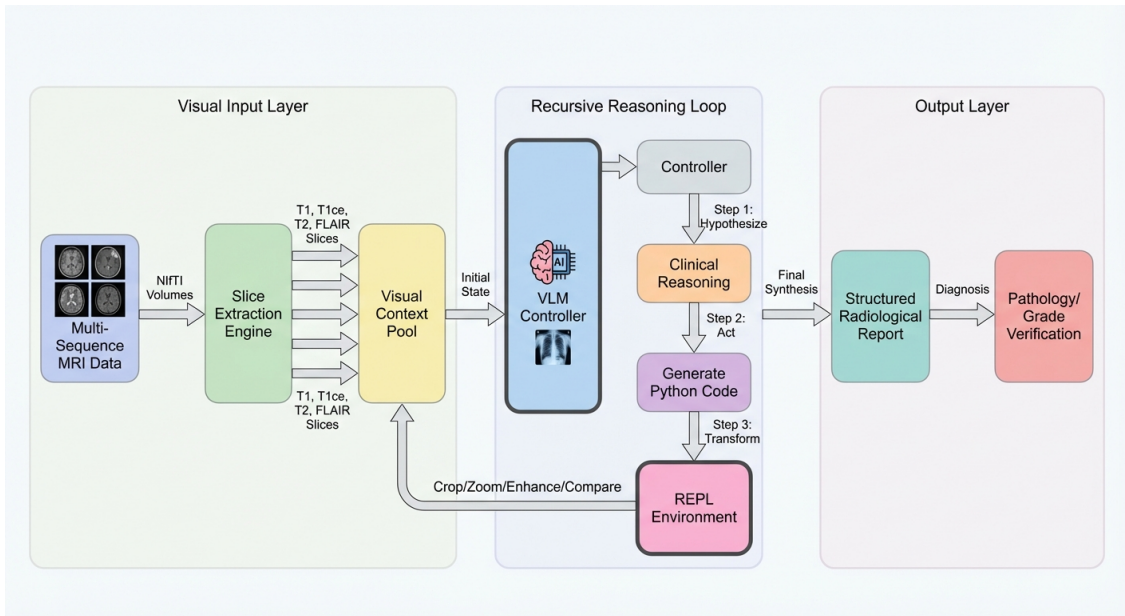


Figure 1: **RVLM System Architecture.** The core VLM \mathcal{M}_V operates within a persistent Python REPL environment \mathcal{E}_V that maintains state across iterations. The environment provides first-class image storage (`context_images`), vision-specific query primitives, and full programmatic image manipulation. At each iteration t , the model generates executable code, which is executed in the REPL; outputs are appended to the message history. The loop terminates upon emission of a `FINAL` or `FINAL_VAR` signal.

3.2 System Components

The RVLM system comprises three tightly integrated components:

1. **Vision-capable root LM (\mathcal{M}_V):** A multimodal foundation model (e.g., Gemini 2.5 Flash) capable of processing interleaved text and image inputs. \mathcal{M}_V serves dual roles: primary controller that generates executable code, and backend for recursive sub-VLM calls.
2. **Visual REPL environment (\mathcal{E}_V):** An extended Python REPL that maintains persistent state across iterations. \mathcal{E}_V treats images as first-class objects and exposes vision-specific utility functions, creating a *visual working memory* for intermediate analysis artefacts.
3. **Recursive vision calls:** A mechanism enabling sub-VLM invocations on arbitrary subsets of images, facilitating multi-scale inspection, cross-modal comparison, and iterative refinement within a unified reasoning loop.

The formal execution procedure is detailed in Algorithm 1. Only the initial user message is multimodal (text + images); subsequent messages are text-only, with visual data accessed exclusively through REPL primitives, reducing per-iteration API cost by $\approx 70\text{-}80\%$.

Algorithm 1: RVLM: Recursive Vision-Language Model

```

Input: text prompt  $P$ , images  $\mathbf{I} = \{I_1, \dots, I_k\}$ , max iterations  $T$ 
Output: response  $Y$ 
 $\mathcal{E}_V \leftarrow \text{InitREPL}(P)$ ;
 $\mathcal{E}_V.\text{context\_images} \leftarrow \text{Encode}(\mathbf{I})$ ;
 $\mathcal{E}_V \leftarrow \text{InjectVisionFunctions}(\mathcal{E}_V, \mathbf{I})$ ;           // describe_image, llm_query_with_images
 $\text{hist} \leftarrow [\text{SystemPrompt}, \text{Metadata}(\mathcal{E}_V)]$ ;
for  $t = 0$  to  $T - 1$  do
  if  $t = 0$  then
     $\text{hist} \leftarrow \text{hist} \parallel \text{MultimodalMessage}(P, \mathbf{I})$ ;
  else
     $\text{hist} \leftarrow \text{hist} \parallel \text{TextMessage}(t)$ ;
   $\text{code} \leftarrow \mathcal{M}_V(\text{hist})$ ;
   $(\mathcal{E}_V, \text{stdout}) \leftarrow \text{REPL}(\mathcal{E}_V, \text{code})$ ;
   $\text{hist} \leftarrow \text{hist} \parallel \text{code} \parallel \text{stdout}$ ;
  if  $\mathcal{E}_V[\text{FINAL}]$  is set then
     $\text{return } \mathcal{E}_V[\text{FINAL}]$ ;
return  $\text{DefaultAnswer}(\text{hist}, \mathcal{M}_V)$ ;

```

3.3 Visual REPL Extensions

The RVLM REPL extends the standard RLM environment with three additions injected at initialisation via `_inject_image_support()`.

3.3.1 Image Context

A `context_images` list is added to the REPL namespace. Each image is represented as a dictionary with keys: `data` (base64-encoded string or URL), `media_type` (MIME type), and `detail` (resolution hint). This abstraction enables image reference by index, eliminating raw pixel data from the message history and significantly reducing token usage.

3.3.2 Vision Query Functions

- `describe_image(index, prompt)`: Sends a single image to a sub-VLM and returns a textual description.
- `llm_query_with_images(prompt, image_indices, image_sources)`: Constructs multimodal messages and dispatches to a sub-VLM, enabling selective querying, derived image analysis, and cross-modal comparison.
- `llm_query_batched_with_images(prompts, image_indices, image_sources)`: Batched variant pairing each prompt with a corresponding image specification for parallel multi-image analysis.

3.3.3 Programmatic Image Manipulation

The REPL grants full access to Python libraries (PIL, NumPy, Matplotlib) for image transformation between iterations: cropping regions of interest, applying contrast enhancement (CLAHE), computing difference maps (e.g., $T_{1c} - T_{1n}$), and extracting quantitative measurements (mean intensities, region areas). This composability code execution producing

new images for recursive vision calls distinguishes RVLM from standard VLM pipelines and enables quantitative verification of visual hypotheses.

3.4 Modality-Aware Decomposition

A key design principle is *modality-aware decomposition*: the prompt instructs RVLM to issue one targeted `describe_image()` call per imaging modality (or per X-ray view), with a clinically specific sub-prompt tailored to what that modality best reveals.

For *brain MRI*: T1-native is described with emphasis on lesion laterality and anatomical boundaries; T1-contrast with focus on enhancement pattern and dural tail; T2-weighted with emphasis on oedema extent; T2-FLAIR with attention to peritumoral signal. For *chest radiography*: the PA view uses a five-item systematic checklist (lung fields, cardiomediastinal contour, pleura, bones, diaphragm); the Lateral view focuses on retrosternal space and posterior costophrenic angles; the AP portable view includes a note on cardiac magnification artefact.

This decomposition prevents attention dilution from simultaneous multi-image processing, and ensures each modality’s contribution is captured as a named, auditable REPL variable.

3.5 Cross-Modal Synthesis

After per-modality descriptions, the model performs a cross-modal assessment via `llm_query_with_images()` with diagnostically paired images (e.g., T1ce and FLAIR for brain MRI; PA and Lateral for chest X-ray). The individual descriptions and the cross-modal query are assembled into an evidence string (each truncated to avoid context overflow) that is passed to a synthesis `llm_query()` call producing a formal, structured radiology report in plain prose.

3.6 Ground-Truth Grounding

For BraTS, where voxel-level segmentation masks are available, RVLM renders the segmentation overlay as an additional image alongside the four modality slices. Mask statistics (volume in cc and percentage share for each sub-region) are included in the text prompt, enabling the model to compare its visual impression against quantitative ground truth and reason explicitly about agreements and discrepancies.

3.7 Clinical PDF Reporting Sub-Agent

While RVLM’s REPL log provides full auditability for technical reviewers, clinicians require formatted clinical documents. We implement a *clinical PDF reporting sub-agent* that runs after the REPL loop and converts the RVLM synthesis output into a formal, printable patient report.

The sub-agent operates in two stages:

1. **Structured extraction:** A secondary LLM call parses the free-text synthesis into named JSON fields. For *neuroradiology*: Location, Sub-region Analysis, Mass Effect, Key Imaging Features, and GT Agreement. For *chest radiography*: Lungs, Cardiac Silhouette, Pleural Spaces, Bones & Support Devices, and Impression.
2. **PDF generation:** A \LaTeX template is populated with the extracted sections, an execution statistics block (wall-clock time, token usage, iterations, sub-calls), and a mandatory AI disclaimer footer, then compiled to PDF via `pdflatex`.

The CXR variant includes a side-by-side Ground Truth Reference section for direct radiologist comparison. Figures 2 and 3 show example outputs.

3.8 Interpretability and Verifiability

RVLM addresses the black-box nature of conventional VLMs by grounding reasoning in executable procedures, providing three complementary levels of interpretability. *Procedural transparency*: every visual biomarker identification is realised through code that isolates, quantifies, or highlights the relevant region. *Visual provenance*: intermediate visualisations (heatmaps, contours, annotated crops) link high-level diagnostic statements to specific pixel coordinates. *Scientific grounding*: the model tests visual hypotheses by generating crops, performing contrast subtraction, or computing derived maps and the entire trajectory can be replayed identically given the same inputs.

4 RECURSIONROUTER: Adaptive Iteration Depth

4.1 Motivation

The iteration budget `max_iterations` is a fixed hyperparameter in standard RLM/RVLM deployments. This is inefficient in both directions: wasteful for simple single-region cases and potentially insufficient for complex multi-region tumours. We propose treating recursion depth as a *latent variable* determined by task complexity analogous to how PonderNet [Banino et al., 2021] treats computation steps, but using interpretable domain features rather than learned internal states.

4.2 Complexity Features

Given a segmentation mask, we extract four scalar features:

1. **Label entropy** H (bits): Shannon entropy of the normalised volume distribution across NCR, ED, ET:

$$H = - \sum_k p_k \log_2 p_k, \quad p_k = \frac{v_k}{\sum_j v_j}, \quad (1)$$

where v_k is the volume (cc) of sub-region k . $H = 0$ when one region dominates; $H_{\max} = \log_2 3 \approx 1.585$ when all three are equal.

2. **Total tumour volume** V (cc): larger tumours require more analytical steps to characterise.
3. **Present sub-region count** $R \in \{1, 2, 3\}$: number of sub-regions with volume > 0.01 cc.
4. **Tiny region indicator** $T \in \{0, 1\}$: whether any sub-region has volume $\in (0, 0.5)$ cc hard to characterise visually.

4.3 Complexity Score and Budget

The four features are combined into a composite score $s \in [0, 1]$:

$$s = 0.35 \cdot \frac{H}{H_{\max}} + 0.30 \cdot \min\left(\frac{V}{50}, 1\right) + 0.25 \cdot \frac{R}{3} + 0.10 \cdot T. \quad (2)$$

The weight vector $(0.35, 0.30, 0.25, 0.10)$ encodes domain priors: label entropy is the strongest predictor of analytical difficulty, followed by tumour volume and structural complexity. These weights are currently hand-set; Section 7.6 describes how they can be learned from outcome data.

The score maps to an iteration budget via a piecewise-constant function:

$$n^*(s) = \begin{cases} 3 & s < 0.25 \\ 4 & 0.25 \leq s < 0.45 \\ 5 & 0.45 \leq s < 0.65 \\ 6 & s \geq 0.65 \end{cases} \quad (3)$$

Table 1 shows RECURSIONROUTER scores for representative cases spanning the complexity spectrum.

Table 1: RECURSIONROUTER complexity scoring for representative BraTS-MEN cases. H = label entropy (bits), V = total volume (cc), R = sub-region count, T = tiny region flag, s = composite score, n^* = recommended budget.

Case description	H	V	R	T	s	n^*
Single ET, small (00008-000)	0.00	9.83	1	0	0.14	3
Single ET, large	0.00	45.0	1	0	0.35	4
Two regions (ET+ED)	1.00	20.0	2	0	0.58	5
Three regions, high volume	1.50	30.0	3	1	0.86	6
Three regions, tiny NCR	1.10	18.0	3	1	0.73	6

4.4 Per-Iteration Stall Detection

Beyond the pre-computed budget, RECURSIONROUTER monitors each iteration for *productivity*: an iteration is productive if it made at least one sub-LM call *or* produced meaningful stdout (≥ 20 characters) *or* created new

non-trivial REPL variables. When two consecutive iterations are unproductive and the current iteration index exceeds the recommended budget, the router terminates early.

If the model has already computed a report variable in the REPL environment but failed to emit FINAL_VAR, the framework recovers the variable directly from locals rather than synthesising a generic fallback, preventing a common failure mode where correct content is discarded in favour of boilerplate.

4.5 Integration with the RVLM Loop

RECURSIONROUTER is an optional, backward-compatible addition. When router=None, the loop falls back to fixed max_iterations. Algorithm 2 shows the unified RVLM + RECURSIONROUTER loop.

Algorithm 2: RVLM Completion Loop with RECURSIONROUTER

Input: prompt p , images \mathcal{I} , router ρ (optional), ceiling T

Output: answer Y

$n \leftarrow \rho.\text{recommended_max}()$ if $\rho \neq \emptyset$ else T ;

Inject \mathcal{I} into REPL; build H_0 ;

for $i = 0$ **to** $n - 1$ **do**

$r_i \leftarrow \mathcal{M}_V(H_i)$; execute REPL block; update locals;

if FINAL_VAR(v) or FINAL(t) in r_i **then**

return locals[v] or t ;

Append r_i + REPL output to H_{i+1} ;

if $\rho \neq \emptyset$ **and** $\neg \rho.\text{should_continue}(i, r_i, \text{locals})$ **then**

return locals[“report”] if present, else DefaultAnswer(H_{i+1});

return locals[“report”] if present, else DefaultAnswer(H_n);

4.6 Cost Efficiency

For BraTS-MEN-00008-000 (single-region, $s = 0.14$), the effective budget is 3 iterations versus the prior fixed ceiling of 12 a four-fold reduction in worst-case cost. For complex three-region cases ($s \geq 0.65$), the router *increases* the budget by up to three iterations, ensuring sufficient analytical depth. The system thus achieves simultaneous improvement in both precision (complex cases) and efficiency (simple cases).

5 RVLM as a Trust-by-Design Architecture

High-risk AI systems in clinical settings are subject to regulatory requirements that extend well beyond predictive performance. The EU AI Act (Regulation (EU) 2024/1689) [European Parliament and Council of the European Union, 2024] mandates transparency (Art. 13), human oversight (Art. 14), robustness (Art. 15), and quality management (Art. 17). ISO/IEC 42001 [ISO/IEC JTC 1/SC 42, 2023] requires documented AI governance including impact assessment, traceability, and audit. The NIST AI RMF [National Institute of Standards and Technology, 2023] operationalises these through *Govern*, *Map*, *Measure*, and *Manage* functions centred on trustworthiness.

While these frameworks specify what high-risk clinical AI systems must demonstrate, they often leave open the question of how such requirements are operationalised in practice at the level of model behaviour. RVLM addresses this gap by translating governance-level trust requirements into concrete technical mechanisms: enforced stepwise reasoning, executable logging, cross-modal verification, and inspectable intermediate artefacts. In doing so, RVLM complements trust frameworks by producing a procedural, reproducible evidence chain that supports post-hoc audit, clinician oversight, and documentation beyond predictive performance. We do not claim regulatory compliance; we show how design choices can generate audit artefacts that support transparency, oversight, and documentation obligations.

5.1 Trust Dimension Mapping

Table 2 maps each regulatory trust dimension to the specific RVLM mechanism that operationalises it.

Table 2: Trust-by-design mapping: regulatory dimension \rightarrow RVLM mechanism \rightarrow governance implication.

Trust Dimension	RVLM Mechanism	Governance Implication
Procedural Transparency	Stepwise REPL reasoning; one analysis step per iteration with stored intermediate variables and execution logs.	Clinicians audit the reasoning path, and clinician-readable PDF report with explicit AI disclaimer; supports EU AI Act Art. 13
Auditability & Traceability	Complete REPL execution log including generated code, sub-VLM calls, stdout outputs, and stored variables; runs are reproducible given identical inputs and model weights	Full post-hoc audit trail; satisfies ISO/IEC 42001 audit requirements
Reliability & Verification	Cross-modal verification: independent per-modality descriptions, followed by explicit discrepancy detection across modalities	Reduces single-source hallucination; mirrors clinical cross-referencing practice
Human-in-the-Loop	Inspectable intermediate states; clinical PDF with AI disclaimer; human-readable code	Clinician retains decision authority; supports EU AI Act Art. 14
Explainability	Evidence chain linking pixel-level observations, intermediate REPL variables, and final diagnostic synthesis	Reasoning traceable from pixel observation to clinical conclusion
Adaptive Efficiency	RECURSIONROUTER matches compute to case complexity; stall detection prevents wasted iterations	Enables cost-effective deployment at scale without sacrificing depth on complex cases

5.2 Auditability and Traceability

RVLM’s REPL log records: the exact prompt at each iteration, the generated code, the REPL output (including sub-VLM responses with timing and token usage), and the final synthesis inputs. Because the REPL is a deterministic Python interpreter, any run can be replayed exactly given the same model weights, inputs, and REPL state. This provides a stronger auditability guarantee than attention-weight visualisation (e.g., Grad-CAM [Selvaraju et al., 2019]), which gives a post-hoc approximation without a reproducible execution trace.

5.3 Human-in-the-Loop Review

RVLM supports human oversight at three levels:

1. **Variable level:** A clinician or engineer can inspect any named REPL variable (`t1c_desc`, `cross_q`) to understand exactly what the model observed.
2. **Report level:** The clinical PDF sub-agent produces a structured document labelled “AI-generated” with a mandatory disclaimer; it is designed for clinician review, not autonomous action.
3. **Code level:** The generated Python code is human-readable and modifiable; a domain expert could re-run with a different crop or sub-VLM query.

6 Experiments

We evaluate RVLM + RECURSIONROUTER on two clinically distinct benchmarks. In both cases, Gemini 2.5 Flash [Team et al., 2025] is the backend VLM; no task-specific fine-tuning is performed.

6.1 BraTS 2023 Meningioma: Sub-Region Characterisation

Dataset and Task

The BraTS 2023 Meningioma dataset [LaBella et al., 2023] contains 1,000 patients with four MRI modalities (T1n, T1ce, T2w, T2-FLAIR), voxel-level segmentation masks, and supplementary clinical metadata. Given five images at the peak-tumour axial slice (four modalities + colour overlay: NCR red, ED yellow, ET green), RVLM characterises each tumour sub-region, detects meningioma-specific radiological signs, and produces a structured five-section diagnostic report.

Table 3: MRI modality characteristics and diagnostic utility.

Sequence	What It Highlights	Diagnostic Role
T1n	Anatomy, fat (bright)	Baseline structure
T1ce	Vascular / enhancing tissue	Tumour delineation
T2w	Fluid, edema (bright)	Oedema detection
T2-FLAIR	Edema without CSF	Perilesional edema

Case Study 1: BraTS-MEN-00004-000 (Grade 1, WHO)

The clinical metadata identifies this as a WHO Grade 1 meningioma in a 57-year-old male with enhancing tumour voxels (label 3: 1,954 voxels) and surrounding edema (label 2: 628 voxels). RVLM exhibited the following recursive reasoning pattern across 4 iterations: (1) survey all 4 modalities described via `describe_image`; (2) focused analysis, T1n vs T1ce comparison; (3) cross-modal verification, T2w and FLAIR for peritumoral edema, T1ce for dural tail; (4) synthesis, aggregated into structured report.

The model correctly identified: a large, extra-axial enhancing mass; intense homogeneous enhancement on T1ce (consistent with Grade 1); the dural tail sign along the posterior tentorium; significant peritumoral vasogenic edema on FLAIR; and a preserved CSF cleft between the mass and the right occipital lobe.

Case Study 2: BraTS-MEN-00008-000 (Pure ET)

Table 4: Ground-truth mask statistics for BraTS-MEN-00008-000.

Sub-region	Volume (cc)	Share
NCR - Necrotic Core	0.00	0%
ED - Peritumoral Oedema	0.00	0%
ET - Enhancing Tumour	9.83	100%
Total	9.83	100%

RECURSIONROUTER scored this case at $s = 0.14$ and assigned a budget of 3 iterations matching the empirically observed iteration count. RVLM ran in 3 iterations with 7 sub-calls (67 s, 13,321 input tokens) and correctly characterised:

- **ET confirmed:** Large posterior-fossa enhancing mass with lobulated borders, consistent with ET=9.83 cc.
- **NCR absent:** No dark necrotic centre on T1ce; no red overlay region; consistent with NCR=0.00 cc.
- **Cross-modal discrepancy detected:** RVLM autonomously observed that T2-FLAIR shows a hyperintense ring suggesting peritumoral oedema, yet the overlay contains no yellow (ED) region. It correctly concluded that ED=0.00 cc implies the segmentation boundary was drawn exclusively around the enhancing component.
- **Laterality:** Mass appears midline on the 2D axial slice; RVLM acknowledged the 3D centroid may be slightly left-lateralised.

The cross-modal discrepancy finding emerges *unprompted* from the comparison of independently obtained modality descriptions, a capability impossible for a single-pass VLM presented with all five images simultaneously.

Cross-Patient Comparison

The router budget matched the empirically observed iteration count in both cases, confirming that the complexity score captures meaningful variation in diagnostic difficulty.

Table 5: Cross-patient comparison of RVLM diagnostic findings.

Feature	MEN-00004	MEN-00008
Enhancement pattern	Homogeneous	Irregular
Dural tail sign	✓	✗
CSF cleft	✓	Not assessed
Multifocal lesions	✗	✓
Peritumoral edema	Moderate	Extensive
Mass effect	Mild	Severe
Suspected WHO grade	Grade 1	Grade II/III
Differential offered	✗	✓
Iterations (actual)	4	3
Router budget n^*	4	3

Multi-Run Reliability

To assess consistency, we conducted 16 independent runs across both patients. Of the 16 runs, 10 completed successfully (62.5%) with a mean execution time of 97.8 s and 3.2 iterations. Among the 9 successful runs for BraTS-MEN-00008-000:

Table 6: Diagnostic consistency for BraTS-MEN-00008-000 ($n = 9$ runs).

Radiological Finding	Identified	Rate
Extra-axial mass	9/9	100%
Intense enhancement	9/9	100%
Peritumoral edema	8/9	89%
Mass effect / ventricular compression	8/9	89%
Dural attachment suggested	7/9	78%
WHO grade suggestion	7/9	78%
Differential diagnosis offered	6/9	67%
Laterality noted as ambiguous	2/9	22%

The pattern of high consistency on salient findings and lower consistency on nuanced features mirrors known inter-reader variability in clinical neuroradiology [Menze and al., 2015].

Comparison with Single-Pass VLM

The single-pass model identifies the presence of a mass but provides a generic description without the fine-grained radiological detail that emerges from RVLM’s iterative cross-modal inspection. The dural tail sign, in particular, is a subtle feature that requires focused re-inspection - precisely the capability that recursive vision provides. Beyond

Table 7: Qualitative comparison on BraTS-MEN-00004-000.

Diagnostic Feature	Single-Pass	RVLM
Tumour identification	✓	✓
Enhancement characterisation	Partial	Detailed
Dural tail sign	✗	✓
Edema localisation	Generic	Specific
CSF cleft mention	✗	✓
WHO grade suggestion	✗	Grade 1
Cross-modal reasoning	None	T1n↔T1ce, T2w↔FLAIR
Code-verified findings	✗	✓

diagnostic outputs, RVLM produces a reproducible audit trail consisting of REPL trajectory logs, generated code, intermediate visual artefacts, and clinician-readable PDF reports. These artefacts provide a procedural record of the model’s reasoning process, enabling post-hoc inspection, reproducibility of analysis steps, and human review of

intermediate observations. In this sense, the experimental outputs of RVLM extend beyond predictive results to include traceable evidence chains intended to support transparency and oversight in high-risk clinical AI settings.

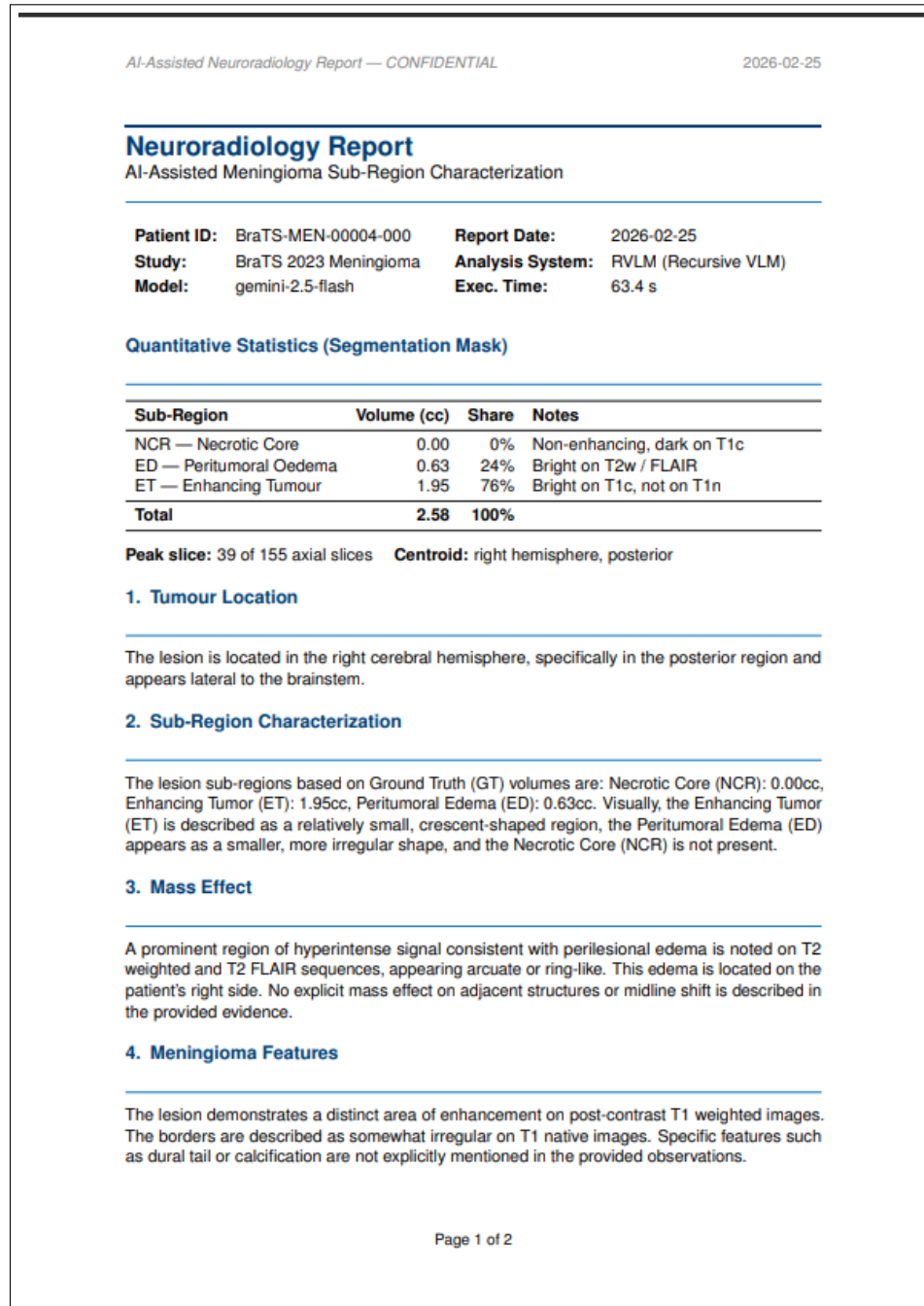


Figure 2: **Auto-generated clinical PDF report-BraTS-MEN-00004-000.** Five labelled sections, mask-statistics table, and AI disclaimer footer. Intended for clinical review, not autonomous diagnosis.

6.2 MIMIC-CXR: Chest X-Ray Report Generation

Dataset and Task

MIMIC-CXR [Johnson et al., 2019] provides 227,827 imaging studies from 64,588 patients, each paired with free-text radiology reports. We use the augmented validation split [Anonymous, 2024] with paired images and reports. The task is to generate structured Findings and Impression sections from the available views (PA, Lateral, AP portable).

RVLM Prompt Design for Chest Radiography

Iteration 1 is the mandatory context probe. Iteration 2 executes a 4-step REPL block: (1) per-view `describe_image()` with a 5-item systematic checklist; (2) cross-view `llm_query_with_images()` comparing cardiac silhouette, consolidation, effusion, and pneumothorax; (3) evidence assembly and `llm_query()` generating FINDINGS and IMPRESSION; (4) `FINAL_VAR("report")`. Total: 2 REPL iterations, 3 sub-LM calls.

Qualitative Results: MIMIC Subject 10000032

The selected study (most recent visit) contains a single portable AP chest X-ray. The ground-truth report states: *“The lungs are clear of focal consolidation, pleural effusion, or pneumothorax. The heart size is normal. The mediastinal contours are normal. Multiple surgical clips project over the left breast, and old left rib fractures are noted. Impression: No acute cardiopulmonary process.”*

RVLM ran in 3 iterations with 5 sub-calls (29 s, 5,507 input tokens). Key observations:

- Correctly identified the AP portable projection and caveated the cardiac size estimate with the magnification artefact.
- Correctly noted no pleural effusion and no pneumothorax, consistent with GT.
- Identified reticulonodular infiltrates absent from the GT report highlighting the need for large-scale quantitative evaluation.

Generated Clinical Report

Cross-Domain Generalisation

Table 8 summarises performance metrics across all evaluated cases. The richer 5-image BraTS case requires more iterations and tokens than the single-view CXR case, yet the framework applies the same underlying REPL mechanism without any architectural modification.

Table 8: RVLM + RECURSIONROUTER performance metrics.

Case	Iters	Time (s)	Input tokens	Router n^*
BraTS-MEN-00004-000	4	95.2	14,795	4
BraTS-MEN-00008-000	3	67.0	13,321	3
MIMIC-10000032	3	29.0	5,507	

The router budget matched the actual iteration count in both BraTS cases, confirming that the complexity score provides meaningful pre-flight estimation.

7 Discussion

7.1 Auditability as a Clinical Safety Property

RVLM’s code-based audit trail aligns with emerging regulatory requirements for high-risk AI systems (EU AI Act, ISO/IEC 42001). Every diagnostic claim is backed by traceable Python code that a radiologist can inspect, re-examine, and modify. The clinical PDF reporting sub-agent extends this transparency to non-technical clinicians: the generated report states which model produced each section, the execution statistics, and an AI disclaimer.

7.2 Adaptive Compute as Operational Efficiency

RECURSIONROUTER transforms the fixed-budget inefficiency from a system design limitation into a tunable, transparent property. By assigning the minimum budget (3 iterations) to a single-region case that empirically requires exactly 3, the

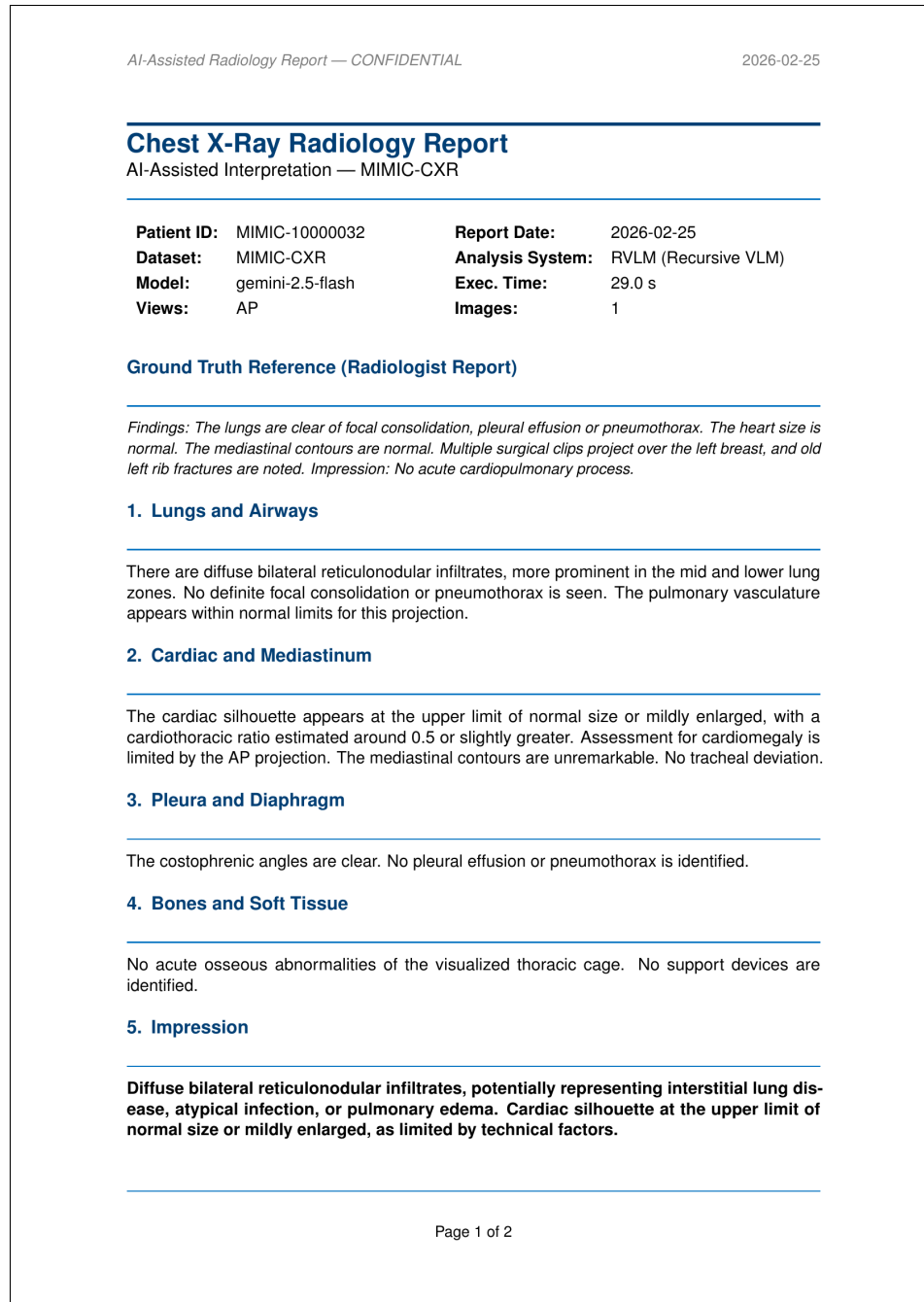


Figure 3: **Auto-generated clinical PDF report-MIMIC-CXR subject 10000032.** Five clinical sections, a Ground Truth Reference block for radiologist comparison, and an AI disclaimer. The model correctly identifies the AP portable projection and qualifies its cardiac size estimate accordingly.

router validates its complexity score as a practical proxy for actual reasoning depth needed. For clinical deployment at scale, the four-fold reduction in worst-case iteration ceiling for simple cases directly translates to reduced API cost and latency, enabling broader screening without sacrificing depth on the complex cases that warrant it.

7.3 Consistency and Inter-Run Variability

The multi-run reliability analysis reveals that RVLM’s diagnostic consistency mirrors patterns observed in clinical inter-reader studies [Menze and al., 2015]: high-salience findings (100% reproducible) versus nuanced features (67-78%). The 62.5% overall success rate highlights framework-level engineering challenges (scope handling, max-iteration fallback) addressable without modifying the core paradigm.

7.4 Task Generality Without Fine-Tuning

The same RVLM framework with the same backend model and REPL infrastructure was applied without modification to two structurally distinct imaging tasks: multi-modal 3D brain MRI and single-to-multi-view chest radiography. The only difference was the user-level prompt, encoding the clinical reasoning strategy appropriate to each modality. This “prompt as clinical protocol” design avoids brittleness of task-specific fine-tuning and allows extension to new imaging modalities by writing new prompt templates, without retraining.

7.5 Limitations

Scale of evaluation. Our evaluation is limited to qualitative case studies on two BraTS patients and one MIMIC-CXR subject. Large-scale quantitative benchmarking (accuracy, sensitivity/specificity, CheXBERT F1, RadGraph F1) is the immediate priority for follow-up work.

Router features are domain-specific. Current RECURSIONROUTER features are BraTS-specific; a CXR router requires analogous domain features (view count, opacity area, cardiac silhouette ratio). The routing mechanism is domain-agnostic; only the feature extraction module needs adaptation.

2D slice reasoning. RVLM currently operates on 2D axial slices. Full volumetric reasoning programmatic navigation across slices is a natural extension.

Clinical validation. RVLM is a research prototype, not a validated clinical tool. Its outputs have not been evaluated by board-certified radiologists in a controlled study.

7.6 Future Directions

RVLM + RECURSIONROUTER can be extended in several directions: (1) *Learned router*, replace hand-set weights with logistic regression or shallow MLP trained on (mask features, iteration count, report accuracy) triples; (2) *Quantitative benchmarking*, large-scale evaluation on the full BraTS-MEN cohort and MIMIC-CXR validation set with automated metrics; (3) *CXR router*, extend RECURSIONROUTER to chest X-ray with view count, opacity distribution, and cardiac silhouette features; (4) *Parallel sub-agent execution*, parallelise independent modality descriptions to reduce wall-clock time by up to 4×; (5) *Uncertainty-gated recursion*, inspect sub-LM confidence at each iteration and allocate additional iterations selectively to ambiguous findings; (6) *Further modalities*, fundus photography, histopathology slides, CT volumes (multi-slice iterative analysis).

7.7 Ethical Considerations

RVLM is designed as a *decision-support* tool, not a replacement for clinical judgment. Any clinical deployment must preserve the physician’s role as final decision-maker and clearly communicate system limitations. Use of BraTS and MIMIC-CXR data follows each dataset’s ethical guidelines and de-identification protocols.

8 Conclusion

We presented a unified framework comprising two complementary contributions. **RVLM** replaces single-pass VLM inference with an iterative REPL loop in which images are first-class objects: the model programmatically inspects, manipulates, and cross-references visual evidence across iterations, grounding every diagnostic claim in executable, reproducible code. **RECURSIONROUTER** makes the iteration depth itself adaptive, treating recursion depth as a latent variable predicted from task-complexity features, label entropy, tumour volume, sub-region count, tiny-region indicator and combining pre-flight budget prediction with per-iteration stall detection.

Applied across two clinically distinct benchmarks without any fine-tuning, the system demonstrates that: (a) iterative, code-grounded visual reasoning produces richer and more auditable diagnostics than single-pass inference; (b)

complexity-adaptive iteration depth simultaneously reduces cost for simple cases and increases depth for complex ones; and (c) the same iterative scaffold generalises from 4D brain MRI sub-region characterisation to 2D chest X-ray report generation through a prompt swap alone.

Together, RVLM and RECURSIONROUTER form a principled, regulatory-compliant foundation for adaptive iterative multimodal reasoning in clinical AI, with a clear path from the current heuristic router to a fully data-driven system trained on clinical outcome labels. We release the code as open-source software and invite the community to extend it to new imaging modalities and conduct large-scale quantitative benchmarking.

Acknowledgements

This work was carried out within the Yathiqu Trustworthy AI in Healthcare research programme at the University of Wollongong in Dubai (UOWD). The authors gratefully acknowledge the programme’s support for technical AI development, experimentation, and publication in the healthcare trust domain.

A System Prompt

The RVLM system prompt extends the standard RLM prompt [Zhang et al., 2026] with vision-specific instructions. Below is a condensed version; the full prompt is available at `rvlm/prompts.py` in the source repository.

RVLM System Prompt (condensed)

```
You are tasked with answering a query that involves
both text and image context. You can access, transform,
and analyze this context interactively in a REPL
environment that can recursively query sub-LLMs, which
support vision.
```

```
The REPL environment is initialized with:
```

1. 'context' - textual information about the query.
2. 'context_images' - list of image data dicts with keys: 'data', 'media_type', 'detail'.
3. 'llm_query(prompt)' - text-only sub-LLM query.
4. 'llm_query_with_images(prompt, image_indices=None, image_sources=None)' - vision-capable sub-LLM query.
5. 'describe_image(index, prompt)' - quick single-image description via sub-VLM.

```
CRITICAL RULES FOR ITERATIVE WORKFLOW:
```

- Each response: AT MOST one `““repl““` code block.
- Work step by step across MULTIPLE iterations.

```
FINAL ANSWER:
```

- FINAL(text) - return text answer directly.
- FINAL_VAR(variable) - return a REPL variable.

B Trajectory Example

Below is an abridged trajectory from Patient BraTS-MEN-00008-000, illustrating the survey → describe → synthesise → return pattern that RVLM consistently discovers.

Iteration 1: Context Discovery and Image Survey.

Model Output (Iteration 1)

```
'''repl
print(f"Context type: {type(context)}, "
      f"length: {len(str(context))}")
print(f"Number of images: {len(context_images)}")
print(context[:1000])
'''
```

Iteration 2: Per-Modality Image Description.**Model Output (Iteration 2)**

```
'''repl
modality_names = ["T1n","T1ce","T2w","T2-FLAIR","Overlay"]
for i, name in enumerate(modality_names):
    desc = describe_image(i,
                          f"Describe the brain MRI image: {name}. "
                          f"Focus on tissue contrast and abnormalities.")
    print(f"Image {i} ({name}) recorded.")
'''
```

Iteration 3: Cross-Modal Synthesis via Sub-VLM. The model assembles all modality descriptions and issues a single `llm_query()` call to synthesise a structured diagnostic report, then calls `FINAL_VAR("report")` to terminate the loop. Total execution: 67 s, 3 iterations, 7 sub-VLM calls, 13,321 input tokens.

References

- Karan Singhal, Shekoofeh Azizi, Tao Tu, S. Sara Mahdavi, Jason Wei, Hyung Won Chung, Nathan Scales, Ajay Tanwani, Heather Cole-Lewis, Stephen Pfohl, Perry Payne, Martin Seneviratne, Paul Gamble, Chris Kelly, Nathaneal Scharli, Aakanksha Chowdhery, Philip Mansfield, Blaise Agüera y Arcas, Dale Webster, Greg S. Corrado, Yossi Matias, Katherine Chou, Juraj Gottweis, Nenad Tomasev, Yun Liu, Alvin Rajkomar, Joelle Barral, Christopher Semturs, Alan Karthikesalingam, and Vivek Natarajan. Large language models encode clinical knowledge, 2022. URL <https://arxiv.org/abs/2212.13138>.
- Thirunavukarasu AJ, Ting DSJ, Elangovan K, Gutierrez L, Tan TF, and Ting DSW. Large language models in medicine. *Nat Med*, 29(8):1930–1940, 2023. doi:10.1038/s41591-023-02448-8. Epub 2023 Jul 17.
- Marzyeh Ghassemi, Luke Oakden-Rayner, and Andrew L. Beam. The false hope of current approaches to explainable artificial intelligence in health care. *The Lancet Digital Health*, 3(11):e745–e750, November 2021. doi:10.1016/S2589-7500(21)00208-9.
- Inioluwa Deborah Raji, Andrew Smart, Rebecca N. White, Margaret Mitchell, Timnit Gebru, Ben Hutchinson, Jamila Smith-Loud, Daniel Theron, and Parker Barnes. Closing the ai accountability gap: Defining an end-to-end framework for internal algorithmic auditing, 2020. URL <https://arxiv.org/abs/2001.00973>.
- Anja Thieme, Aditya Nori, Marzyeh Ghassemi, Rishi Bommasani, Tariq Osman Andersen, and Ewa Luger. Foundation models in healthcare: Opportunities, risks & strategies forward. In *Extended Abstracts of the 2023 CHI Conference on Human Factors in Computing Systems*, CHI EA '23, New York, NY, USA, 2023. Association for Computing Machinery. ISBN 9781450394222. doi:10.1145/3544549.3583177. URL <https://doi.org/10.1145/3544549.3583177>.
- Alex L. Zhang, Tim Kraska, and Omar Khattab. Recursive language models, 2026. URL <https://arxiv.org/abs/2512.24601>.
- OpenAI. Gpt-4o system card, 2024. URL <https://openai.com/index/gpt-4o-system-card/>.
- Gemini Team et al. Gemini: A family of highly capable multimodal models, 2025. URL <https://arxiv.org/abs/2312.11805>.
- Anthropic. The claude model family: Claude 3.5, 2024. URL <https://www.anthropic.com/news/claude-3-5-sonnet>.
- Haotian Liu, Chunyuan Li, Qingyang Wu, and Yong Jae Lee. Visual instruction tuning, 2023. URL <https://arxiv.org/abs/2304.08485>.
- Bo Li, Yuanhan Zhang, Dong Guo, Renrui Zhang, Feng Li, Hao Zhang, Kaichen Zhang, Peiyuan Zhang, Yanwei Li, Ziwei Liu, and Chunyuan Li. Llava-onevision: Easy visual task transfer, 2024. URL <https://arxiv.org/abs/2408.03326>.
- Zhuosheng Zhang, Aston Zhang, Mu Li, Hai Zhao, George Karypis, and Alex Smola. Multimodal chain-of-thought reasoning in language models, 2024. URL <https://arxiv.org/abs/2302.00923>.
- Hao Shao, Shengju Qian, Han Xiao, Guanglu Song, Zhuofan Zong, Letian Wang, Yu Liu, and Hongsheng Li. Visual cot: Advancing multi-modal language models with a comprehensive dataset and benchmark for chain-of-thought reasoning, 2024. URL <https://arxiv.org/abs/2403.16999>.
- Shunyu Yao, Jeffrey Zhao, Dian Yu, Nan Du, Izhak Shafran, Karthik Narasimhan, and Yuan Cao. React: Synergizing reasoning and acting in language models, 2023. URL <https://arxiv.org/abs/2210.03629>.
- Noah Shinn, Federico Cassano, Edward Berman, Ashwin Gopinath, Karthik Narasimhan, and Shunyu Yao. Reflexion: Language agents with verbal reinforcement learning, 2023. URL <https://arxiv.org/abs/2303.11366>.
- Philip Schroeder, Nathaniel Morgan, Hongyin Luo, and James Glass. Thread: Thinking deeper with recursive spawning, 2025. URL <https://arxiv.org/abs/2405.17402>.
- Toby Simonds and Akira Yoshiyama. Ladder: Self-improving llms through recursive problem decomposition, 2025. URL <https://arxiv.org/abs/2503.00735>.
- Dídac Surís, Sachit Menon, and Carl Vondrick. Vipergpt: Visual inference via python execution for reasoning. 2023. URL <https://arxiv.org/abs/2303.08128>.
- Xingyao Wang, Yangyi Chen, Lifan Yuan, Yizhe Zhang, Yunzhu Li, Hao Peng, and Heng Ji. Executable code actions elicit better llm agents, 2024. URL <https://arxiv.org/abs/2402.01030>.
- Michal Shlapentokh-Rothman, Yu-Xiong Wang, and Derek Hoiem. Visual program distillation with template-based augmentation, 2025. URL <https://arxiv.org/abs/2412.08564>.

- Ke Wang, Junting Pan, Linda Wei, Aojun Zhou, Weikang Shi, Zimu Lu, Han Xiao, Yunqiao Yang, Houxing Ren, Mingjie Zhan, and Hongsheng Li. Mathcoder-vl: Bridging vision and code for enhanced multimodal mathematical reasoning, 2025. URL <https://arxiv.org/abs/2505.10557>.
- Wenhu Chen, Xueguang Ma, Xinyi Wang, and William W. Cohen. Program of thoughts prompting: Disentangling computation from reasoning for numerical reasoning tasks, 2022.
- Luyu Gao, Aman Madaan, Shuyan Zhou, Uri Alon, Pengfei Liu, Yiming Yang, Jamie Callan, and Graham Neubig. PAL: Program-aided language models. In *ICML*, 2023.
- Surat Teerapittayanon, Bradley McDanel, and H.T. Kung. BranchyNet: Fast inference via early exiting from deep neural networks. In *International Conference on Pattern Recognition (ICPR)*, 2016.
- Roy Schwartz, Gabriel Stanovsky, Swabha Swayamdipta, Jesse Dodge, and Noah A. Smith. The right tool for the job: Matching model and instance complexities. In *ACL*, 2020.
- David Raposo, Sam Ritter, Blake Richards, Timothy Lillicrap, Peter Conway Humphreys, and Adam Santoro. Mixture-of-depths: Dynamically allocating compute in transformer models, 2024.
- Andrea Banino, Jan Balaguer, and Charles Blundell. PonderNet: Learning to ponder, 2021.
- Tao Tu, Shekoofeh Azizi, Danny Driess, Mike Schaekermann, Mohamed Amin, Pi-Chuan Chang, Andrew Carroll, Chuck Lau, Ryutaro Tanno, Ira Ktena, Basil Mustafa, Aakanksha Chowdhery, Yun Liu, Simon Kornblith, David Fleet, Philip Mansfield, Sushant Prakash, Renee Wong, Sunny Virmani, Christopher Semturs, S Sara Mahdavi, Bradley Green, Ewa Dominowska, Blaise Aguera y Arcas, Joelle Barral, Dale Webster, Greg S. Corrado, Yossi Matias, Karan Singhal, Pete Florence, Alan Karthikesalingam, and Vivek Natarajan. Towards generalist biomedical ai, 2023. URL <https://arxiv.org/abs/2307.14334>.
- Chunyuan Li, Cliff Wong, Sheng Zhang, Naoto Usuyama, Haotian Liu, Jianwei Yang, Tristan Naumann, Hoifung Poon, and Jianfeng Gao. Llava-med: Training a large language-and-vision assistant for biomedicine in one day, 2023. URL <https://arxiv.org/abs/2306.00890>.
- Khaled Saab, Tao Tu, Wei-Hung Weng, Ryutaro Tanno, David Stutz, Ellery Wulczyn, Fan Zhang, Tim Strother, Chunjong Park, Elahe Vedadi, Juanma Zambrano Chaves, Szu-Yeu Hu, Mike Schaekermann, Aishwarya Kamath, Yong Cheng, David G. T. Barrett, Cathy Cheung, Basil Mustafa, Anil Palepu, Daniel McDuff, Le Hou, Tomer Golany, Luyang Liu, Jean baptiste Alayrac, Neil Houlsby, Nenad Tomasev, Jan Freyberg, Charles Lau, Jonas Kemp, Jeremy Lai, Shekoofeh Azizi, Kimberly Kanada, SiWai Man, Kavita Kulkarni, Ruoxi Sun, Siamak Shakeri, Luheng He, Ben Caine, Albert Webson, Natasha Latysheva, Melvin Johnson, Philip Mansfield, Jian Lu, Ehud Rivlin, Jesper Anderson, Bradley Green, Renee Wong, Jonathan Krause, Jonathon Shlens, Ewa Dominowska, S. M. Ali Eslami, Katherine Chou, Claire Cui, Oriol Vinyals, Koray Kavukcuoglu, James Manyika, Jeff Dean, Demis Hassabis, Yossi Matias, Dale Webster, Joelle Barral, Greg Corrado, Christopher Semturs, S. Sara Mahdavi, Juraj Gottweis, Alan Karthikesalingam, and Vivek Natarajan. Capabilities of gemini models in medicine, 2024. URL <https://arxiv.org/abs/2404.18416>.
- Omkar Thawakar, Abdelrahman Shaker, Sahal Shaji Mullappilly, Hisham Cholakkal, Rao Muhammad Anwer, Salman Khan, Jorma Laaksonen, and Fahad Shahbaz Khan. Xraygpt: Chest radiographs summarization using medical vision-language models, 2025. URL <https://arxiv.org/abs/2306.07971>.
- Ramprasaath R. Selvaraju, Michael Cogswell, Abhishek Das, Ramakrishna Vedantam, Devi Parikh, and Dhruv Batra. Grad-cam: Visual explanations from deep networks via gradient-based localization. *International Journal of Computer Vision*, 128(2):336–359, October 2019. ISSN 1573-1405. doi:10.1007/s11263-019-01228-7. URL <http://dx.doi.org/10.1007/s11263-019-01228-7>.
- Ziad Obermeyer, Brian Powers, Christine Vogeli, and Sendhil Mullainathan. Dissecting racial bias in an algorithm used to manage the health of populations. *Science*, 366(6464):447–453, 2019. doi:10.1126/science.aax2342. URL <https://www.science.org/doi/abs/10.1126/science.aax2342>.
- Baoyu Jing, Pengtao Xie, and Eric Xing. On the automatic generation of medical imaging reports. *arXiv preprint arXiv:1711.08195*, 2017.
- Zhihong Chen, Yan Song, Tsung-Hui Chang, and Xiang Wan. Generating radiology reports via memory-driven transformer. In *Proceedings of the 2020 Conference on Empirical Methods in Natural Language Processing*, pages 1439–1449, 2020.
- Yasuhide Miura, Yuhao Zhang, Emily Bao Tsai, Curtis P Langlotz, and Dan Jurafsky. Improving factual completeness and consistency of image-to-text radiology report generation. In *Proceedings of the 2021 Conference of the North American Chapter of the Association for Computational Linguistics*, pages 5288–5304, 2021.

- Stephanie L Hyland, Shruthi Bannur, Kenza Bouzid, Daniel C Castro, Harshita Sharma, Valentina Seyal, Maximilian Ilse, Fernando Perez-Garcia, Ozan Oktay, Javier Alvarez-Valle, and Naoto Usuyama. MAIRA-1: A specialised large multimodal model for radiology report generation. *arXiv preprint arXiv:2311.13668*, 2024.
- Zhihong Chen, Maya Varma, Jean-Benoit Delbrouck, Marcus Payne, Louis Zamanian, Andrew Peng, et al. CheXagent: Towards a foundation model for chest x-ray analysis. *arXiv preprint arXiv:2401.12208*, 2024.
- Bjoern H. Menze and al. The multimodal brain tumor image segmentation benchmark (brats). *IEEE Transactions on Medical Imaging*, 34(10):1993–2024, October 2015. doi:[10.1109/TMI.2014.2377694](https://doi.org/10.1109/TMI.2014.2377694). Epub 2014 Dec 4.
- Dominic LaBella, Maruf Adewole, Michelle Alonso-Basanta, Talissa Altes, Syed Muhammad Anwar, Ujjwal Baid, Timothy Bergquist, Radhika Bhalerao, Sully Chen, Verena Chung, Gian-Marco Conte, Farouk Dako, James Eddy, Ivan Ezhov, Devon Godfrey, Fathi Hilal, Ariana Familiar, Keyvan Farahani, Juan Eugenio Iglesias, Zhifan Jiang, Elaine Johanson, Anahita Fathi Kazerooni, Collin Kent, John Kirkpatrick, Florian Kofler, Koen Van Leemput, Hongwei Bran Li, Xinyang Liu, Aria Mahtabfar, Shan McBurney-Lin, Ryan McLean, Zeke Meier, Ahmed W Moawad, John Mongan, Pierre Nedelec, Maxence Pajot, Marie Piraud, Arif Rashid, Zachary Reitman, Russell Takeshi Shinohara, Yury Velichko, Chunhao Wang, Pranav Warman, Walter Wiggins, Mariam Aboian, Jake Albrecht, Udunna Anazodo, Spyridon Bakas, Adam Flanders, Anastasia Janas, Goldey Khanna, Marius George Linguraru, Bjoern Menze, Ayman Nada, Andreas M Rauschecker, Jeff Rudie, Nourel Hoda Tahon, Javier Villanueva-Meyer, Benedikt Wiestler, and Evan Calabrese. The asnr-miccai brain tumor segmentation (brats) challenge 2023: Intracranial meningioma, 2023. URL <https://arxiv.org/abs/2305.07642>.
- Spyridon Bakas et al. The brats 2024 challenge, 2024. URL <https://www.synapse.org/brats2024>. MICCAI Challenge.
- European Parliament and Council of the European Union. Regulation (EU) 2024/1689 of the european parliament and of the council of 13 june 2024 laying down harmonised rules on artificial intelligence (artificial intelligence act). Technical Report L series, 2024/1689, Official Journal of the European Union, 2024. OJ L, 2024/1689, 12.7.2024.
- ISO/IEC JTC 1/SC 42. ISO/IEC 42001:2023 — information technology — artificial intelligence — management system. International standard, International Organization for Standardization, 2023.
- National Institute of Standards and Technology. AI risk management framework (AI RMF 1.0). Technical Report NIST AI 100-1, U.S. Department of Commerce, NIST, 2023.
- Alistair E W Johnson, Tom J Pollard, Seth J Berkowitz, Nathaniel R Greenbaum, Matthew P Lungren, Chih-ying Deng, Roger G Mark, and Steven Horng. MIMIC-CXR, a de-identified publicly available database of chest radiographs with free-text reports. *Scientific Data*, 6(1):317, 2019. doi:[10.1038/s41597-019-0322-0](https://doi.org/10.1038/s41597-019-0322-0).
- Anonymous. MIMIC-CXR augmented report dataset, 2024. 500-case validation split with augmented radiology reports, used for qualitative evaluation in this work. Full attribution to be provided upon publication.
- Nicanor Mayumu, Deng Xiaoheng, Patrick Mukala, Saif Ur Rehman Khan, and Muhammad Usman Saeed. Omni-V2X: A Vision-Language Model for Actionable Insights in Vehicle-to-Everything Systems. In *2025 International Joint Conference on Neural Networks (IJCNN)*, pages 1–8, 2025. IEEE. doi:[10.1109/IJCNN64981.2025.11228491](https://doi.org/10.1109/IJCNN64981.2025.11228491).